CMS Physics Analysis Summary

Contact: cms-future-conveners@cern.ch 2017/05/29

Projected performance of Higgs analyses at the HL-LHC for ECFA 2016

The CMS Collaboration

Abstract

Projections of 13 TeV Higgs boson analyses to the High-Luminosity LHC conditions, with an integrated luminosity of up to 3000 fb^{-1}, are presented. The studies are performed under two scenarios, considering the systematic uncertainties in the present and in the High-Luminosity LHC conditions. The performance of $H \to ZZ$, $H \to \gamma\gamma$, HH and beyond the standard model $H \to \tau\tau$, and $H \to$ invisible are shown.

1 Introduction

The discovery of a Higgs boson in 2012 by the ATLAS and CMS collaborations [1–3] opened a new era of precise measurements of the properties of the new particle, aimed to thoroughly test its consistence with the standard model (SM) predictions. The LHC is currently the only machine capable of producing on-shell Higgs bosons. The data collected by the LHC experiments during Run-I and the beginning of Run-II has already provided important measurements of Higgs boson properties, and the list of results will increase through the LHC program. The present measurements of the Higgs boson couplings to fermions, bosons and of the tensor structure of the Higgs boson interaction with electroweak gauge bosons show no significant deviations with respect to the SM expectations.

However, the current LHC data alone cannot fully probe all the observables necessary to characterize the boson. An outstanding example is the measurement of the trilinear self-coupling. This measurement, that can be performed using events containing a Higgs boson pair, will directly probe the Higgs field potential. As the cross section for double Higgs production is expected to be very small in the SM, a large data sample is needed to probe this process. A similar requirement of high statistics is found in other precision measurements, such as the CP behavior of the boson, its fiducial cross section, or measurements in rare decay channels. A precise determination of the Higgs couplings to fundamental particles, to the percent level, may allow to discriminate between SM predictions and new physics models. A direct exploration of extended Higgs sectors, through the search for additional Higgs bosons, will also strongly benefit from a larger data set.

The high luminosity LHC (HL-LHC) will provide a unique opportunity to thoroughly test the Higgs boson properties. The instantaneous luminosity will increase substantially, allowing to collect 3000 fb^{-1} by the end of the HL-LHC program and leading to more than 140 additional interactions per bunch crossing, denoted as pileup (PU), which could significantly affect the performance of the analyses. In addition, the CMS detector will be significantly affected by radiation damage by the time of the HL-LHC. For this reason, a series of upgrades are planned to recover the detector performance compromised by radiation damage and increased PU. These upgrades, and their expected effect on the performance of the CMS detector are described in detail in the Technical Proposal for the Phase-II Upgrade of the CMS Detector [4].

CMS reported the expected sensitivity of various Higgs boson analyses at the HL-LHC in [4, 5], based on projections of 8 TeV measurements using 2012 CMS data, and DELPHES [6] simulation studies performed in 2014, incorporating the Phase-II detector upgrades. The studies summarized here repeat and complement the previous public results at 300 fb^{-1} and 3000 fb^{-1}, updating the corresponding analyses techniques to their current status.

The document is organized as follows. Section 2 contains a description of the extrapolation scenarios employed. Section 3 summarizes the projections of the $\text{H} \to \gamma\gamma$ measurements, including a study on the impact of precision timing in the upgraded detector. Section 4 follows with the description of the $\text{H} \to \text{ZZ}$ projections. In section 5, current results on projected uncertainties for the $\text{H} \to \gamma\gamma$ and $\text{H} \to \text{ZZ}$ signal strengths are compared to previous CMS results. A study of Higgs boson pair production in several final states is shown in Section 6, where both projections of the current searches and a first study of $\text{HH} \to \text{WW}qq$ with DELPHES are shown. Finally, Sections 7 and 8 are dedicated to BSM searches: projections for the search for a Higgs boson of the minimal supersymmetric standard model (MSSM) [7, 8] decaying into τ leptons and invisible decays of a Higgs boson ($\text{H} \to \text{inv.}$) produced via vector boson fusion.

2 Systematic uncertainties assumed for extrapolation

The results summarized in this report are based on CMS public measurements performed on the 13 TeV 2015 and early 2016 proton-proton data sets, projected to larger data sets of 300 and 3000 fb^{-1} assuming $\sqrt{s} = 13$ TeV, for the European Committee for Future Accelerators (ECFA) 2016 workshop.

The pileup conditions at the HL-LHC will be far more challenging than those faced in current analyses. In addition, there is the effect of radiation damage on the CMS detector, especially the endcaps. A series of upgrades are planned to reduce these two effects, but degradation in analysis performance is possible.

In order to summarize the future physics potential of the CMS detector at the HL-LHC, the projections are presented under different scenarios assumed for the size of systematic uncertainties, which are expected to bracket a realistic extrapolation. The baseline scenarios assume that the CMS upgrades will provide the same level of detector and trigger performance as in the 2015/2016 data taking period [4]. The incorporation of the performance of the upgraded detectors and the effect of higher pileup conditions are labeled with a + sign:

- **ECFA S1 :** All systematic uncertainties are kept constant with integrated luminosity. The performance of the CMS detector is assumed to be unchanged with respect to the reference analysis;
- **ECFA S1+ :** All systematic uncertainties are kept constant with integrated luminosity. The effects of higher pileup conditions and detector upgrades on the future performance of CMS are taken into account [4];
- **ECFA S2 :** Theoretical uncertainties are scaled down by a factor 1/2, while experimental systematic uncertainties are scaled down by the square root of the integrated luminosity until they reach a defined lower limit based on estimates of the achievable accuracy with the upgraded detector. The effects of higher pileup conditions and detector upgrades on the future performance of CMS are not taken into account;
- **ECFA S2+ :** Theoretical uncertainties scaled down by a factor 1/2, while experimental systematic uncertainties are scaled down by the square root of the integrated luminosity until they reach a defined lower limit based on estimates of the achievable accuracy with the upgraded detector. The effects of higher pileup conditions and detector upgrades on the future performance of CMS are taken into account [4].

The incorporation of the performance of the upgraded detectors and the effect of higher pileup conditions in the ECFA16 S1+ and S2+ scenarios are additions upon the scenarios employed in [5]. A more detailed explanation of the Snowmass 2013 S1 and S2 scenarios is given in Section 5.

Systematic uncertainties in triggering, selection, and identification efficiencies for electrons and muons are expected to be reduced to 1%, and are assumed to be fully correlated between leptons of the same flavour. Hadronic τ lepton (τ_h) performance is assumed to be similar to the current one, and a lower bound of half the current uncertainty in their identification and isolation efficiency is assumed for scenario S2. Uncertainty in the jet energy scale (JES) is expected to reach the 1% precision for jets with $p_T > 30$ GeV. The missing transverse energy uncertainty is obtained by propagating the JES uncertainties in its computation. The current missing transverse energy performance is assumed for these projections, thanks to detector improvements and improved pile-up rejection techniques. Identification for b-tagged jets is expected to improve to achieve a minimum of 1% (2%) uncertainty in the selection efficiency of b (c) quarks,

and of 2%-10% of uncertainty in misidentifying a light jet. The uncertainty in the integrated luminosity of the data sample could be reduced down to 1.5% by a better understanding of the calibration and fit models employed in its determination, and making use of the finer granularity and improved electronics of the upgraded detectors.

Prompt photon identification in the high pileup environment of the HL-LHC was studied in detail in [4]. The performance of the upgraded CMS detector for photon isolation efficiency, photon resolution and vertex-finding efficiency has been taken into account in the upgraded S1+ and S2+ scenarios. Contamination due to additional noise interactions coming from pileup interactions in the detector can worsen isolation efficiency. We apply an estimated reduction of 2.3% (10%) in identification efficiency for prompt photons in the barrel (endcaps), for both signal and background events, in scenarios S1+ and S2+. The photon energy resolution could also be affected by the contamination of isolation variables at the HL-LHC. However, the planned upgrades to the CMS detector will maintain the current performance [4]. Therefore, no worsening of the photon resolution has been considered in the extrapolation. High pileup can also lead to a drop in vertex-finding efficiency. This impacts the invariant mass resolution of diphoton pairs. The current vertex-finding efficiency value, 80%, is assumed unchanged in S1 and S2. S1+ and S2+ assume a pessimistic scenario in which the efficiency has been worsened to 40%. Dedicated studies have been performed to show the mitigation of this degradation with precision timing, and are described in Section 3.1.

Theoretical uncertainties follow the prescriptions of the LHC Yellow Report 4 [9] in S1 and S1+. In S2 and S2+ they are halved to account for future theoretical developments.

3 $\mathrm{H} \to \gamma\gamma$

The CMS experiment has released an updated measurement of a Higgs boson decaying into two photons using the 2016 data set [10]. The analysis is based on 12.9 fb^{-1} of data collected at $\sqrt{s} = 13$ TeV. The analysis provided measurements of Higgs boson properties, namely the signal strength μ (inclusively and for the Higgs production modes ggH, ttH and VBF), and the fiducial cross section (σ_{fid}). This section presents an extrapolation to the conditions of the HL-LHC with 3000 fb^{-1} of data, in order to estimate how well the observables above could be measured by the end of the HL-LHC program. It should be noted that this CMS Higgs to diphoton analysis does not have specific event categories targeting the associated vector boson Higgs (VH) production mode. Consequently, no extrapolation for μ_{VH} is provided.

Projected symmetrized uncertainties for the $\mathrm{H} \to \gamma\gamma$ signal strength relative to the standard model ($\mu^{\gamma\gamma}$), inclusively and per production mode (labeled "VBF", "ttH" and "ggH") are shown in Fig. 1, and numerically in Table 1.

The projected relative uncertainties for the $\mathrm{H} \to \gamma\gamma$ fiducial cross section are shown in Fig. 2 and Table 2. The fiducial volume is defined on generator-level quantities, with the following requirements on lead (γ_1) and sublead (γ_2) photons: $p_{\mathrm{T}}^{gen}(\gamma_1) > 1/3\, m_{\gamma\gamma}$, $p_{\mathrm{T}}^{gen}(\gamma_2) > 1/4\, m_{\gamma\gamma}$; $|\eta^{gen}(\gamma_{1(2)})| < 2.5$; the isolation of the photons ($\mathrm{Iso}_{R=0.3}^{gen}(\gamma_{1(2)})$), calculated as the sum of the transverse momenta of all stable particles inside a cone of aperture R=0.3 around the photon, is required to be less than 10 GeV.

Projections are given for integrated luminosities of 300 fb^{-1} and 3000 fb^{-1} in the previously described scenarios. For the 3000 fb^{-1} case the effect of the high pileup conditions of the HL-LHC has been taken into account as degradations to the photon identification efficiency and vertex identification efficiency. In each case the uncertainty in the inclusive signal strength

is also given split in components: statistical uncertainties ("stat."), experimental systematic uncertainties ("exp.") and theoretical systematic uncertainties ("theo."). In scenarios S2 and S2+, the experimental systematics uncertainties are dominated by luminosity, reduced to 1.5%, and JES.

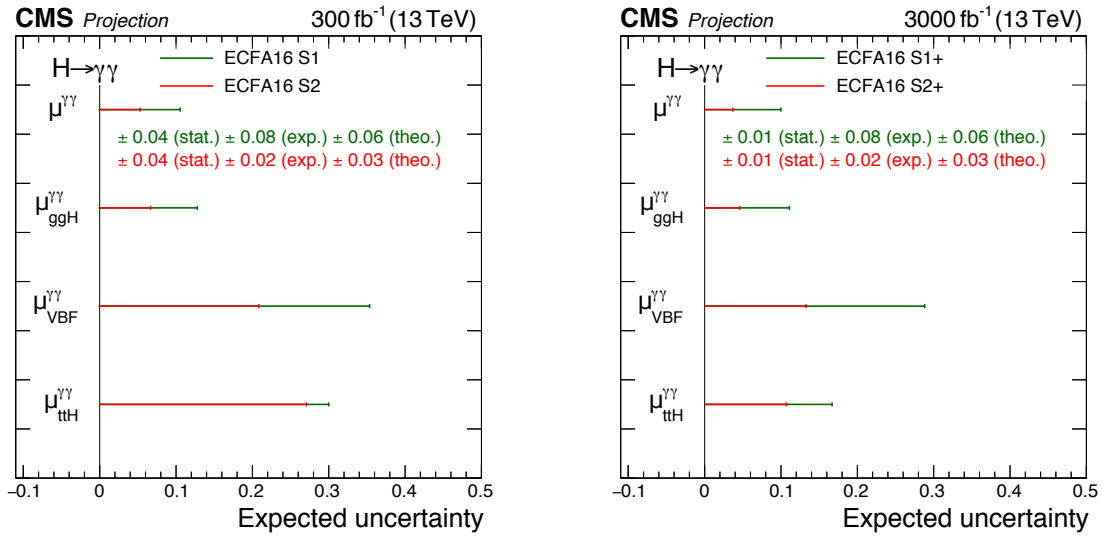

(a) (b)

Figure 1: Projected symmetrized uncertainties for the H $\to \gamma\gamma$ signal strength relative to the standard model, inclusively and per production mode. Projections are given for 300 fb^{-1} (a) and 3000 fb^{-1} (b), under the scenarios described in the text.

Table 1: Projected symmetrized uncertainties for the H $\to \gamma\gamma$ signal strength relative to the standard model, inclusively and per production mode. The inclusive signal strength is also given split in components: statistical uncertainties ("stat."), experimental systematic uncertainties ("exp.") and theoretical systematic uncertainties ("theo."). Projections are given for 300 fb^{-1} and 3000 fb^{-1}, under the scenarios described in the text.

Projected uncertainty in the H $\to \gamma\gamma$ signal strength (%)				
	300 fb^{-1}		3000 fb^{-1}	
	ECFA16 S1	ECFA16 S2	ECFA16 S1+	ECFA16 S2+
$\mu^{\gamma\gamma}_{\mathrm{ggH}}$	13	7	11	5
$\mu^{\gamma\gamma}_{\mathrm{VBF}}$	35	21	29	13
$\mu^{\gamma\gamma}_{\mathrm{ttH}}$	30	27	17	11
3 $\mu^{\gamma\gamma}$	11	5	10	4
	(stat.) $\pm$ (exp.) $\pm$ (theo.)			
$\mu^{\gamma\gamma}$	$4 \pm 8 \pm 6$	$4 \pm 2 \pm 3$	$1 \pm 8 \pm 6$	$1 \pm 2 \pm 3$

3.1 Timing studies

Existing planned upgrades to the barrel Electromagnetic Calorimeter electronics and cooling in the central region, as well as the High Granularity Calorimeter in the forward region may

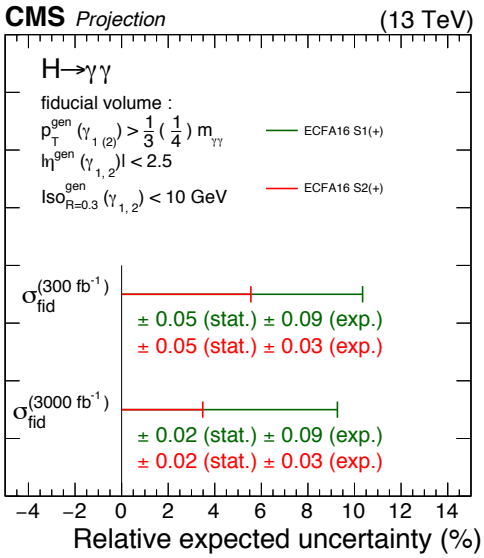

Figure 2: Projected relative uncertainties for the H $\to \gamma\gamma$ fiducial cross section. Projections are given for 300 fb^{-1} and 3000 fb^{-1}, under the scenarios described in the text.

Table 2: Projected relative uncertainties for the H $\to \gamma\gamma$ fiducial cross section. Projections are given for 300 fb^{-1} and 3000 fb^{-1}, under the scenarios described in the text.

Projected relative uncertainty in σ_{fid} (%)		
300 fb^{-1}	ECFA16 S1	$5(\text{stat.}) \pm 9(\text{exp.})$
	ECFA16 S2	$5(\text{stat.}) \pm 3(\text{exp.})$
3000 fb^{-1}	ECFA16 S1+	$2(\text{stat.}) \pm 9(\text{exp.})$
	ECFA16 S2+	$2(\text{stat.}) \pm 3(\text{exp.})$

provide precision timing capabilities for the high energy photons from H $\to \gamma\gamma$ decays in the calorimeter. Global event timing is also being considered as a possible extension to the Phase-II upgrade program through additional subdetectors, which provide precision timing measurements for charged particles in order to improve pileup suppression in primary vertex reconstruction, isolation, jets, and missing energy.

Studies of the effect of precision timing capabilities for photons and charged particles on the H $\to \gamma\gamma$ primary vertex selection have been carried out in [11]. These indicate that for H $\to \gamma\gamma$ events with sufficiently large rapidity separation between the photons, corresponding to about 50% of the event sample, the primary vertex position can be located with precision timing for the photons alone with a precision of around 1 cm. The small rapidity separation for the remaining events does not allow a useful determination of the vertex location without additional information. These studies also show that, by combining the photon timing with precision timing for tracks and primary vertices, the effective amount of pileup is reduced by a factor of five.

Four scenarios are compared. In the first scenario "S2", no degradation due to higher pileup is applied, and therefore the present 2016 performance of $\sim$ 80% primary vertex selection efficiency is retained. In the "S2+ Pessimistic" scenario, degradation of performance is applied corresponding to 140 PU conditions, such that the primary vertex selection efficiency is reduced

to 40%. An additional 5% reduction in efficiency affecting both the signal and irreducible background is included, in order to account for degraded photon identification performance in the high pileup conditions. Additional variations of the S2+ scenario are also shown. The "S2+ intermediate" scenario corresponds to the case where precision timing is available for the photons from the calorimeters, and therefore a 5x reduction in the effective pileup is assumed for 50% of the events, corresponding to the sample with $|\Delta\eta_{\gamma\gamma}| > 0.8$, and the total vertex selection efficiency is therefore increased to 55%. In the final "S2+ Optimistic" scenario, precision timing is assumed to be available both for the photons in the calorimeters, as well as for the charged particles in the event. In this case a 5x reduction in the effective pileup is assumed for all of the events, and the total primary vertex selection efficiency is increased to 75%, nearly fully recovering the present 2016 performance. The signal lineshape and projected uncertainty in the fiducial cross section measurement for the four scenarios are shown in Fig. 3. The improvement from precision timing moving from the pessimistic to optimistic scenario corresponds to approximately 15% reduction in the statistical uncertainty of the fiducial cross section measurement.

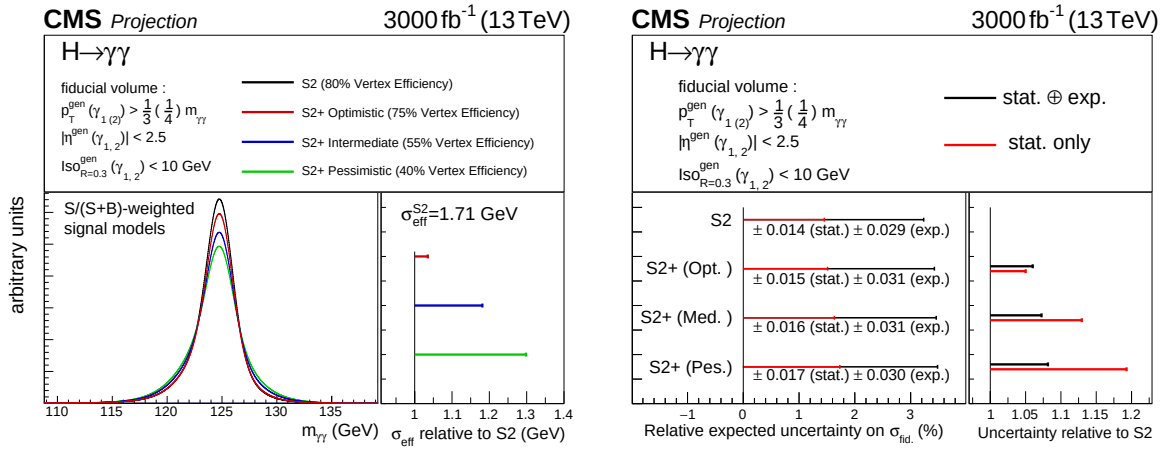

Figure 3: (a) Lineshape for $H \to \gamma\gamma$ signal in each of the four considered scenarios. Since this is a combination over several analysis categories, the individual category contributions are weighted according to the signal to background ratio in order to be representative of their contribution to the final result. (b) Projected uncertainty in the fiducial cross section measurement for 3000 fb^{-1} of integrated luminosity for each of the four scenarios. The inset on the right shows the total and statistical uncertainty relative to the scenario maintaining 2016 performance.

4 $H \to ZZ$

Projections for the $H \to ZZ \to 4\ell$ decay channel have been obtained by scaling the signal and background yields of the 2016 analysis which used 12.9 fb^{-1} of data [12]. In this section scenarios S1 and S2 are considered for the projections to 300 fb^{-1}. Projections to 3000 fb^{-1} are made under scenarios S1+ and S2+.

In scenarios S2 and S2+ the experimental uncertainties in the integrated luminosity and the lepton identification efficiency are reduced to 1.5% and 1% per lepton, respectively, fully correlated between all leptons of the same flavour. In the S1+ and S2+ cases, signal and background yields are adjusted to take into account effects of an upgraded detector and higher pileup according to studies in [4].

Results on the projected signal strengths per production mode at 300 and 3000 fb^{-1} are shown in Fig. 4. Table 3 lists the values shown in the figure. For the subleading production modes, the uncertainties are dominated by the statistical component in both S1 and S2 scenarios. In each case the uncertainty in the inclusive signal strength is shown split into three components: statistical uncertainties ("stat."), experimental systematic uncertainties ("exp.") and theoretical systematic uncertainties ("theo."). At 3000 fb^{-1}, the experimental systematics uncertainties, dominated by luminosity, JES, and lepton efficiencies, are slightly constrained due to the nature of the fit to the $m_{4\ell}$ sidebands. Theoretical uncertainties also show a small constrain as a result of the background theoretical uncertainty, which is correlated with the signal one.

The projection of the differential cross section measurement as a function of the transverse momentum of the Higgs boson is shown in Fig. 5. In this measurement, the theoretical uncertainties in the total signal cross section are not relevant and the cross section is measured in a fiducial phase space closely matching the experimental acceptance [12]. In this measurement the high p_T region ($p_T > 200$ GeV) is still dominated by the statistical uncertainty at 3000 fb^{-1}. The statistical uncertainty of the measurements ranges from 10 to 29% (4 to 9%) for 300 (3000) fb^{-1}.

Anomalous contributions in the spin-0 tensor structure of HZZ interactions can be characterized by coefficients a_2, a_3, Λ_1, and Λ_Q defined in Refs. [13, 14]. The contribution to the total cross section from these coefficients can be parametrized in terms of their fractional contribution to on-shell HZZ decay via the fractions f_{ai} and phases ϕ_{ai} [13, 14]. Only tensor structures proportional to a_2, a_3 and Λ_1 are observable using on-shell H boson decay. The extrapolations for these couplings are performed using the 4ℓ channel following the techniques described in Refs. [12, 13], in terms of $f_{ai} \times cos(\phi_{ai})$ with the assumption $\phi_{ai} = 0$ or π.

Results are visualized in Fig. 6 as the projected 95% confidence level (CL) intervals at 300 fb^{-1} for scenario S1 and 3000 fb^{-1} for scenario S1+. Table 4 lists the values shown in the figure. Since the measurement is statistically limited, only scenarios S1 and S1+, where the systematic uncertainties are unchanged with respect to the reference analysis, are shown.

Table 3: Projected symmetrized uncertainties for the H $\rightarrow$ ZZ signal strength relative to the standard model, inclusively and per production mode. The inclusive signal strength is also given split in components: statistical uncertainties ("stat."), experimental systematic uncertainties ("exp.") and theoretical systematic uncertainties ("theo."). Projections are given for 300 fb^{-1} and 3000 fb^{-1}, under the scenarios described in the text.

Projected uncertainty in H $\rightarrow$ ZZ signal strength (%)				
	300 fb^{-1}		3000 fb^{-1}	
	ECFA16 S1	ECFA16 S2	ECFA16 S1+	ECFA16 S2+
μ^{ZZ}_{ggH}	12	9	9	5
μ^{ZZ}_{VBF}	39	39	17	16
μ^{ZZ}_{VH}	71	71	26	25
μ^{ZZ}_{ttH}	81	81	32	31
μ^{ZZ}	11	7	8	5
	(stat.) $\pm$ (exp.) $\pm$ (theo.)			
$\mu^{\gamma\gamma}$	$5 \pm 7 \pm 7$	$5 \pm 4 \pm 4$	$2 \pm 4 \pm 7$	$2 \pm 3 \pm 3$

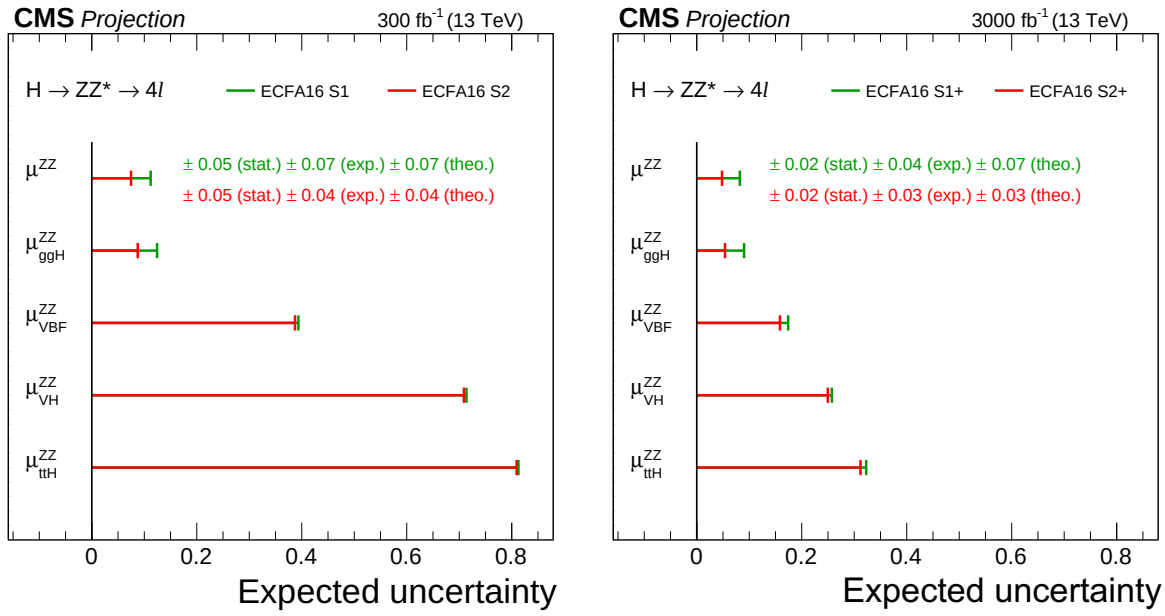

(a) (b)

Figure 4: The projected 68% CL uncertainties in the Higgs boson signal strength for different production modes at 300 fb^{-1} (a) and 3000 fb^{-1} (b), with S1(+) in green and S2(+) in red.

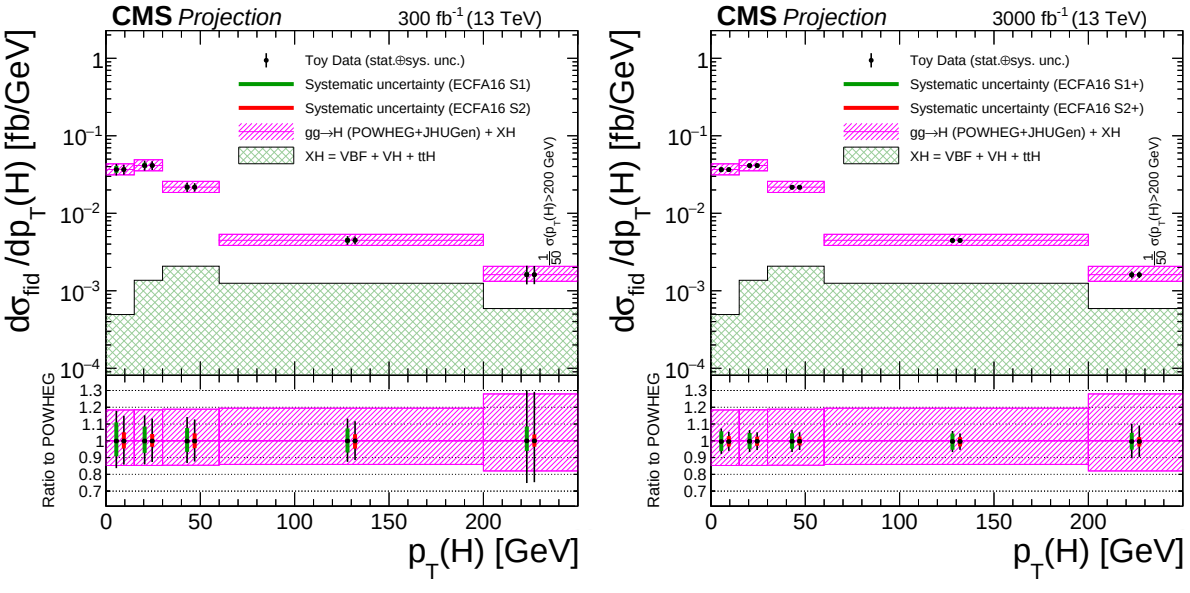

(a) (b)

Figure 5: Projections for the differential fiducial cross section measurement of the Higgs boson transverse momentum at 300 fb^{-1} (a) and 3000 fb^{-1} (b). The theoretical uncertainty in the differential gluon fusion cross section, which does not affect the measurement, is taken at NLO and shown in magenta. The statistical uncertainty of the measurement ranges from 10 to 29% (4 to 9%) for 300 (3000) fb^{-1}. The last bin represents the integrated cross section for $p_T(H)$ >200 GeV and is scaled by 50 for presentation.

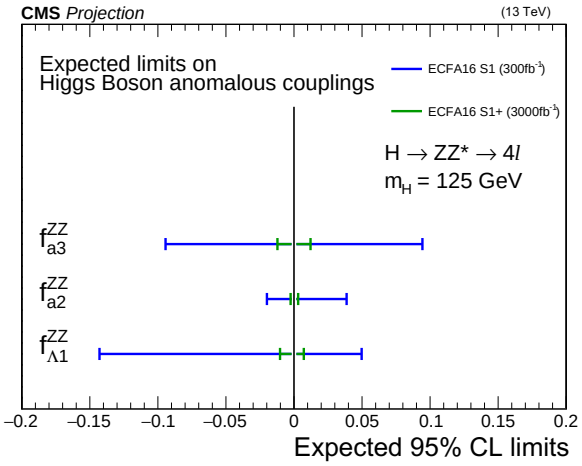

Figure 6: The projected 95% CL values of $f_{ai} \times cos\,(\phi_{ai})$ at 300 fb^{-1} and 3000 fb^{-1}. Since the measurement is statistically limited, only S1 (for 300 fb^{-1}) and S1+ (for 3000 fb^{-1}) scenarios are used.

Table 4: The projected 95% CL values of $f_{ai} \times cos\,(\phi_{ai})$ at 300 fb^{-1} and 3000 fb^{-1}. Since the measurement is statistically limited, only scenario 1 where the systematic uncertainties are unchanged with respect to the reference analysis is shown. The limits do not scale exactly with integrated luminosity because the interference contribution becomes more dominant at smaller values of $f_{ai} \times cos\,(\phi_{ai})$, and because the projections for 3000 fb^{-1} use different lepton efficiencies and misidentification rates to account for the higher pileup at the HL-LHC as described in Section 2.

Parameter	300 fb^{-1}	3000 fb^{-1}
$f_{a3} \times cos\,(\phi_{a3})$	[-0.094, 0.094]	[-0.012, 0.012]
$f_{a2} \times cos\,(\phi_{a2})$	[-0.020, 0.039]	[-0.0025, 0.0031]
$f_{\Lambda 1} \times cos\,(\phi_{\Lambda 1})$	[-0.14, 0.05]	[-0.010, 0.0072]

5 Comparison ECFA16 vs Snowmass13 results

Projected uncertainties for the H $\to \gamma\gamma$ and H $\to$ ZZ $\to 4\ell$ signal strengths, as shown in Figs. 4 and 1, compared to those from the Snowmass report [5], are shown in Fig. 7.

The Snowmass13 S1 and Snowmass13 S2 scenarios are those defined for the Snowmass13 conference, and differ from their ECFA16 counterparts in several aspects. The detector and pileup effects for the HL-LHC were not accounted for in Snowmass13. No lower bounds for experimental systematics were put in place when scaling with integrated luminosity. The assumed theoretical uncertainties differ between the two projections and are taken from Yellow Report 3 [15] for Snowmass13 and Yellow Report 4 [9] for ECFA16. Finally, the projections were done for a center-of-mass energy of 14 TeV in Snowmass13, and of 13 TeV in ECFA16.

6 Double Higgs boson production

6.1 SM HH production

Searches for non-resonant HH final state which used 2015 data, with integrated luminosities ranging from 2.3 to 2.7 fb^{-1}, are extrapolated to estimate the ultimate sensitivity of the CMS

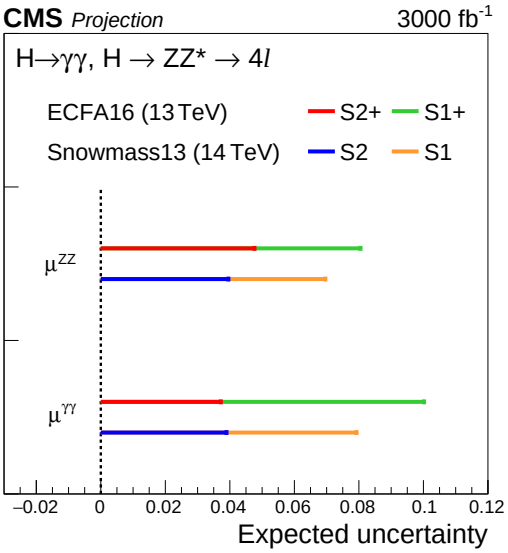

Figure 7: Comparison between the projections obtained in the ECFA16 and Snowmass13 studies for the $H \to \gamma\gamma$ and $H \to ZZ \to 4\ell$ projected uncertainties in signal strengths. Projections are given for 3000 fb^{-1} under the scenarios described in the text.

experiment with a sample of 3000 fb^{-1} of data collected at the end of the HL-LHC run. We provide projections for the four final states currently under scrutiny by the CMS collaboration: HH $\to \gamma\gamma$bb [16], HH $\to \tau\tau$bb [17], HH $\to$ 4b [18] as well as HH $\to VV$bb [19], the latter looking at the $llv\nu$bb final state with $l = e, \mu$.

The extrapolations presented in this document assume $\sqrt{s} = 13\,\text{TeV}$. At this center-of-mass energy the predicted SM HH ggF production cross section is $33.41^{+7.3\%}_{-8.4\%}$ fb for $m_\text{H} = 125.09\,\text{GeV}$ [9]. However, the nominal center-of-mass energy at the HL-LHC is $\sqrt{s} = 14\,\text{TeV}$ with a predicted cross section of 39.51 fb, corresponding to an increase in cross section by 18%. Assuming a background scaling of $14/13 \approx 1.08$, the projected results are expected to underperform by $1.18/\sqrt{1.08} \approx 15\%$ with respect to the HL-LHC energy conditions.

Estimates of the CMS performance [4] at the HL-LHC are considered to perform the projections of the results. Uncertainties in the JES and on the identification of jets originating from b quarks are assumed to be 1% at the time of the HL-LHC. Other uncertainties are specific of the analyses and therefore detailed per channel:

- HH $\to \gamma\gamma$bb: Photon efficiencies and uncertainties are treated in the same way as for the H $\to \gamma\gamma$ projection described in Section 3. Since 90% of the photons coming from HH decays are in the central part of the detector, the larger photon efficiency degradation in the forward region of the detector is neglected.
- HH $\to \tau\tau$bb: The current uncertainty in the shape of the $\text{t}\bar{\text{t}}$ prediction is scaled down by a factor three to match the the estimated fraction of jets faking τ leptons [4] at the HL-LHC. The QCD multijet background is subdominant and obtained from data and therefore the statistical uncertainty is assumed to be negligible. The μ, e and τ_h uncertainties are assumed to be unchanged compared to the 2015 analysis.
- HH $\to VV$bb: The main backgrounds, $\text{t}\bar{\text{t}}$ and Drell-Yan processes, are expected to be estimated from data and therefore their uncertainties are considered to be negligible.
- HH $\to$ 4b: The main background, QCD multijet production, is estimated from data

and its uncertainty is scaled down with the integrated luminosity in the projection. The uncertainties in the predictions of the other backgrounds are assumed to be unchanged with respect to the 2015 analysis.

The results of the projections, which assume S2 scenario on the systematic uncertainties and a scenario without systematic uncertainties shown to assess their impact (Stat. Only), are shown in Table 5. For the gg $\rightarrow$ HH $\rightarrow$ $\gamma\gamma$bb case the S2+ scenario was used. The uncertainty in the signal strength is also shown in Fig. 8(a). Results of the HH $\rightarrow$ VVbb channel are in good agreement with those obtained in previous studies [4], based on the simulated CMS upgraded detector.

In the case of the HH $\rightarrow$ $\gamma\gamma$bb channel, results of the current projections at 13 TeV are slightly worse than the previous ones that were obtained at 14 TeV [4]. Both analysis are based on the usage of a two-dimensional method for the extraction of the signal, with the variables m_{bb} and $m_{\gamma\gamma}$. The difference in performance of the projection presented here is driven by a background estimation based on 2015 data instead of Monte Carlo simulation, the center-of-mass energy considered and the single Higgs background sources included. It is known since Ref. [4] that the single Higgs background has a significant impact on the gg $\rightarrow$ HH $\rightarrow$ $\gamma\gamma$bb channel sensitivity. This contribution was already considered in the 8 TeV analysis [20], but in 13 TeV analysis based on 2015 data its impact was neglected as it was expected to be negligible. Therefore we additionally included five different single Higgs production mechanisms in our projection: ggH, VBF, VH, ttH and the associated production with two b quarks. In Ref [4] different selections were proposed to reduce the ttH contribution: events with isolated leptons as well as a large number of additional jets were rejected. In this projection we assumed that 50% of the ttH background, expected in Ref [20] selection, could be rejected in this way, keeping the signal efficiency nearly unchanged. All other contributions were left unchanged. A degradation of 13% was observed on the total uncertainty on the SM HH production measurement when the SM single Higgs contribution was included compared to a pure extrapolation from Ref [16].

In the case of the HH $\rightarrow$ $\tau\tau$bb channel, the difference in the projected sensitivity with respect to previous results [4, 21] comes from the different assumptions made in each of the projections. In particular, the previous projection uses the DELPHES framework to simulate the CMS detector response and assumes that the multijet background is completely rejected thanks to a 60 GeV threshold on the τ lepton transverse momentum, significantly higher than the 45 GeV thresholds used in Run-II analyses. While the current analysis uses only the mass as final discriminating variable, the previous analysis uses a more optimal BDT which exploits the power of many different discriminating variables and their correlations. The combination of these effects results in a better S/B ratio and consequently in a better sensitivity. On the other hand, the preliminary results [17] used for the current projection to an integrated luminosity of 3000 fb^{-1} have a significant contribution from multijet background, as well as a higher contamination from the $t\bar{t}$ process that limit their sensitivity. The rejection of both background contributions is expected to improve once more data is available to constrain them.

A projection of the sensitivity to the SM HH $\rightarrow$ $\tau\tau$bb production as function of the integrated luminosity is shown in Fig. 8(b).

6.2 Resonant HH production

The search for resonant $X \rightarrow$ HH production, based on 13 TeV analysis performed with data collected in 2015 [22], is projected to an integrated luminosity of 3000 fb^{-1} in the HH $\rightarrow$ 4b channel. Three masses of the X resonance are considered, m_X = 300 GeV, 700 GeV and 1000 GeV.

Table 5: Projection of the sensitivity to the SM gg $\rightarrow$ HH production at 3000 fb^{-1} expected to be collected during the HL-LHC program. The projections are based on 13 TeV analysis performed with data collected in 2015. The median expected limit, Z-value and uncertainty in the signal modifier $\mu_r = \sigma_{\mathrm{HH}}/\sigma_{\mathrm{SMHH}}$ are provided assuming S2 scenario on the systematic uncertainties and a scenario without systematic uncertainties shown to assess their impact (Stat. Only). For gg $\rightarrow$ HH $\rightarrow \gamma\gamma$bb we use S2+ scenarios and we include the single Higgs contribution to the background.

	Median expected limits in μ_r		Z-value		Uncertainty as fraction of $\mu_r = 1$	
Channel	ECFA16 S2	Stat. Only	ECFA16 S2	Stat. Only	ECFA16 S2	Stat. Only
gg $\rightarrow$ HH $\rightarrow \gamma\gamma$bb (S2+)	1.44	1.37	1.43	1.47	0.72	0.71
gg $\rightarrow$ HH $\rightarrow \tau\tau$bb	5.2	3.9	0.39	0.53	2.6	1.9
gg $\rightarrow$ HH $\rightarrow VV$bb	4.8	4.6	0.45	0.47	2.4	2.3
gg $\rightarrow$ HH $\rightarrow$ bbbb	7.0	2.9	0.39	0.67	2.5	1.5

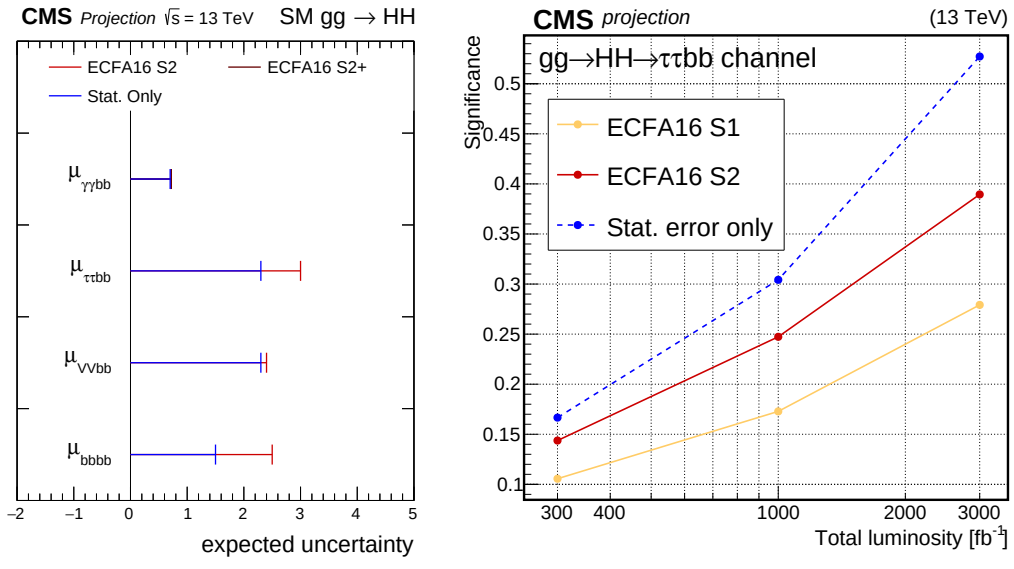

(a) (b)

Figure 8: (a) Projection of the sensitivity to the SM gg $\rightarrow$ HH production at 3000 fb^{-1}, based on 13 TeV preliminary analyses performed with data collected in 2015. The uncertainty in the signal modifier $\mu = \sigma/\sigma_{\mathrm{SM}}$ is provided assuming different scenarios on the systematic uncertainties. (b) Projection of the sensitivity to the SM HH $\rightarrow \tau\tau$bb production as function of the collected luminosity, based on the 13 TeV preliminary analysis [17] performed with data collected in 2015, under different assumptions on the systematic uncertainties.

We consider a spin-0 hypothesis for which we assume a radion production cross section within Bulk WED theory [23]. The radion (R) [24–27] is an additional element of WED models that is needed to stabilize the size of the extra dimension l. It is usual to express the benchmark points of the model in terms of the dimensionless quantity $k/\overline{M}_{\mathrm{Pl}}$, and the mass scale $\Lambda_{\mathrm{R}} = \sqrt{6}\exp[-kl]\overline{M}_{\mathrm{Pl}}$, with the latter interpreted as the ultraviolet cutoff of the model [28]. From the expected limit, we obtain the value of Λ_{R} at which the radion is excluded with masses of 300, 700 and 1000 GeV.

The results of the projections, under two different uncertainty scenarios, are shown in Table 6. For each resonant mass the theoretically predicted value at NLO for radion production with the mass scale $\Lambda_{\mathrm{R}} = \sqrt{6}\exp[-kl]\overline{M}_{\mathrm{Pl}} = 1$ TeV is indicated both in the text and in the table caption. The cross section exclusion is translated into the exclusion on Λ_{R} at 95% CL.

Table 6: Projection of the sensitivity to $gg \to X \to HH \to bbbb$ production at 3000 fb^{-1} expected to be collected during the HL-LHC program. The 95% CL expected limits are provided for spin-0 resonance hypothesis with different mass assumptions.

	Median expected limits on σ (fb)		$\sigma_{\mathrm{R}}^{NLO}(\Lambda_{\mathrm{R}} = 1\,\mathrm{TeV})$ (fb)	Λ_{R} (TeV) excluded
m_X(TeV)	ECFA16 S2	Stat. Only		ECFA16 S2
0.3	46	41	7130	13
0.7	7.3	3.4	584	8.9
1.0	4.4	2.4	190	6.6

6.3 $HH \to bbWW \to bbqql\nu$ at HL-LHC

The study of the $HH \to bbWW \to bbqql\nu$ production considers the CMS Phase-II detector simulation instead of projecting an existing CMS result to the HL-LHC conditions. The energy of the collisions is assumed to be $\sqrt{s} = 14$ TeV with mean PU interactions of 200. The integrated luminosity considered for the study is 3000 fb^{-1}. The DELPHES fast simulation framework [6] is used to model the Phase-II detector. The parametrized performance of the Phase-II detector in DELPHES is taken from the corresponding GEANT-based [29] full simulation samples.

For a cross section of 40 fb, 8640 bbqqlν signal events from $HH \to bbWW$ decays, are expected at the end of the HL-LHC run. The dominant background process is $t\bar{t}$ production with semi-leptonic decay yielding a factor $\sim 10^5$ more events than signal. Other backgrounds have negligible contribution in comparison to $t\bar{t}$ and only the dominant $t\bar{t}$ background is considered. Selected events are required to have 2 b-tagged jets with $p_{\mathrm{T}} > 30$ GeV and $|\eta| < 2.5$, at least four jets with $p_{\mathrm{T}} > 20$ GeV and $|\eta| < 2.5$, exactly one lepton with $|\eta| < 2.5$, $p_{\mathrm{T}} > 25$ GeV for electrons, $p_{\mathrm{T}} > 20$ GeV for muons, and missing transverse energy $E_{\mathrm{T}}^{\mathrm{miss}} > 20$ GeV. Contributions from pileup interactions to jets are removed using the PUPPI algorithm [30, 31].

A boosted decision tree (BDT) based on kinematic properties of the events is used as final discriminant. The BDT takes into account the correlation among the input variables. The signal selection is obtained by applying a threshold on the BDT discriminator leading to 68.1 signal events and 8696 background events.

From these results, expected 95% CL upper limits on the σ/σ_{SM} are derived using the asymptotic approximation of the modified frequentist approach based on the $\mathrm{CL_s}$ criterion. This analysis assumes that the signal yield has a systematic uncertainty of 10% originating from the PDF and scale uncertainties [32]. The resulting upper limit on σ/σ_{SM} is evaluated as a function of

the systematic uncertainty in the background from 0 to 5%, as shown in Fig. 9 (a). The expected relative uncertainty in signal strength versus background systematic uncertainty is shown in Fig. 9 (b).

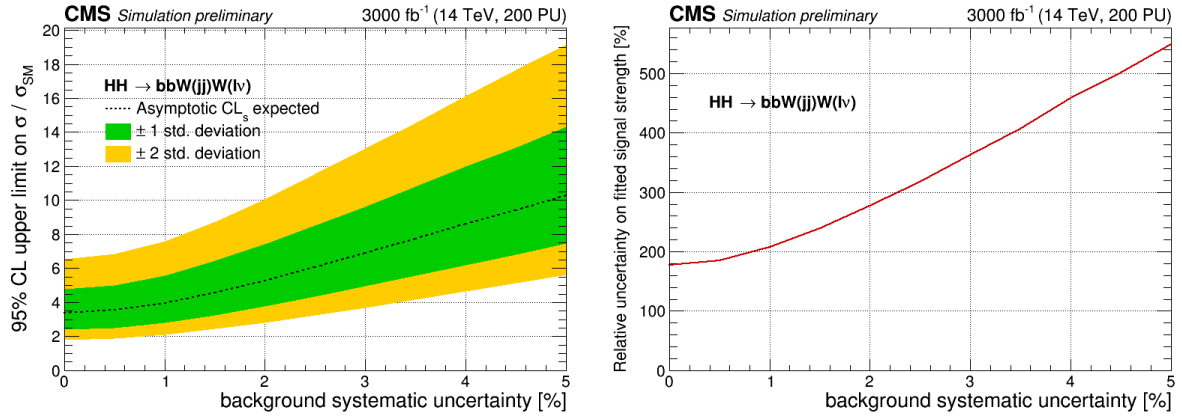

(a) (b)

Figure 9: (a) The expected 95% upper limit on σ/σ_{SM} versus background systematic uncertainty. This was determined with the asymptotic approximation of the modified frequentist approach based on the CLs criterion by assuming a 10% systematic uncertainty in the signal originating from PDF and scale uncertainty. (b) The expected relative uncertainty in signal strength as a function of the background systematic uncertainty.

7 MSSM $\phi \to \tau\tau$

The Higgs sector of the MSSM consists of two Higgs doublets, one of which couples to up-type and one to down-type fermions. This results in five physical Higgs particles: two charged $H^{\pm}$, one neutral pseudoscalar A and two neutral scalars h and H (note that the three neutral Higgs bosons are often denoted $\phi = h, H, A$). Generally, allowed MSSM scenarios incorporate the 125 GeV Higgs boson as the lighter scalar h and are parametrized at tree level using the quantities m_A, the mass of the pseudoscalar Higgs boson, and $\tan\beta$, the ratio of vacuum expectation values of the two Higgs doublets. The (often large) radiative corrections are typically fixed based on experimentally and phenomenologically sensible choices for the SUSY parameters, each choice defining a particular "benchmark scenario". The di-τ lepton final state provides the most sensitive direct search for additional Higgs bosons predicted by the MSSM for high values of $\tan\beta$, due to the enhanced coupling to down-type fermions.

The results of searches for MSSM $\phi \to \tau\tau$ are interpreted in two different ways. In the most "model-independent" case a single resonance signal for a Higgs boson in the mass range between 90 GeV to 3.2 TeV, and decaying into τ leptons is searched for, setting upper limits on cross section times branching fraction for each of the two dominant production modes in the MSSM: gluon fusion (ggϕ) and b associated production (bbϕ). In the more "model-dependent" case a limit is set as a function of m_A and $\tan\beta$ in a particular MSSM benchmark scenario, combining the prediction from both production modes and all three neutral Higgs bosons. Both results are based on the same analysis, in which the following final states of the two τ leptons are considered: $\mu\tau_h$, $e\tau_h$, $\tau_h\tau_h$ and $e\mu$. The dominant irreducible background is from Drell-Yan production with a decay to τ lepton pairs, with other important backgrounds coming from W+jets, $t\bar{t}$, and QCD multijet production, in which one or both selected τ leptons originate

from misidentified jets. Events are separated into those which contain at least one b tagged jet and those which contain no b tagged jets, targeting bbϕ and ggϕ production respectively. The final discriminant which is fitted for signal extraction is the transverse di-τ lepton mass.

The projections to 300 and 3000 fb^{-1} are based on a recent public version of this analysis, performed using 2.3 fb^{-1} of data taken during 2015, at a center of mass energy of $\sqrt{s} = 13$ TeV [33].

The S1 and S2 scenarios are considered and limits are also evaluated assuming only statistical uncertainties (Stat. Only). In S2, the minimum uncertainties in the electron and muon efficiencies are 1%; the uncertainties in the τ lepton identification efficiency, which vary depending on the di-τ lepton decay channel and the τ p_{T}, are reduced by a half at most; and the b tagging efficiency uncertainty has a minimum of 1%. Theoretical uncertainties, affecting both signal and background predictions, are assumed to be reduced by a factor 2 with respect to the present ones. The systematic uncertainty in integrated luminosity reaches a minimum of 1.5 %.

The projected model-independent limits for these two scenarios are given in Fig. 10. The limits are given for integrated luminosities of 300 fb^{-1} and 3000 fb^{-1}, and are compared with the expected limits from the 2015 data set analysis with 2.3 fb^{-1}. The difference in expected limit between the two scenarios reduces with increasing m_{ϕ}. This reflects the smaller relative importance of the systematic uncertainties in limiting the sensitivity at higher masses, where the background expectation is small.

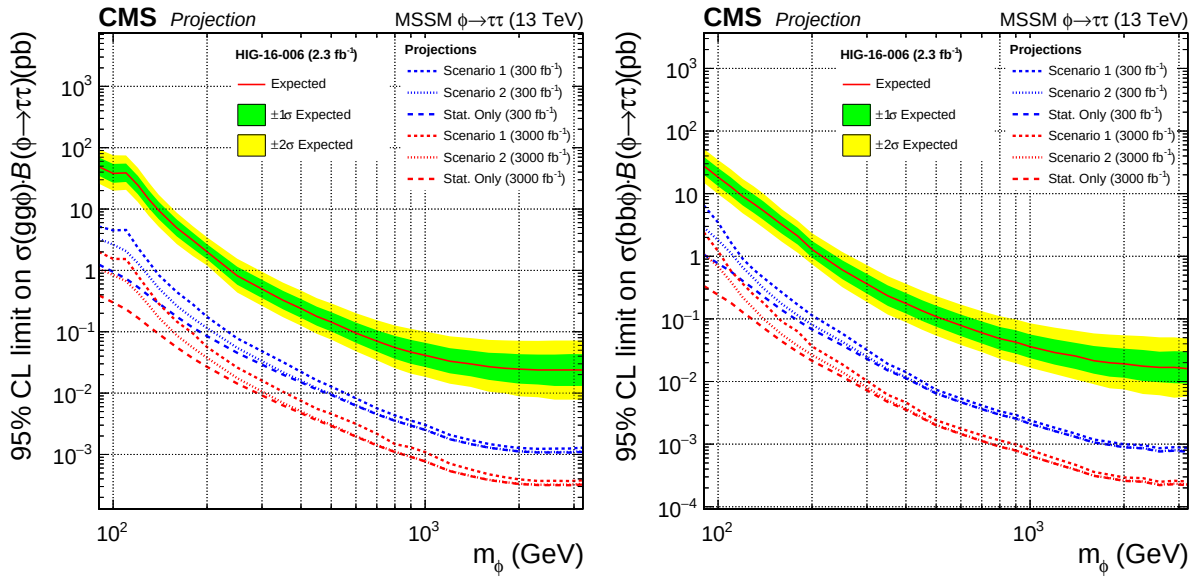

(a) (b)

Figure 10: Projected 95% CL upper limits on the cross section times branching fraction for the production of a neutral Higgs boson in the gluon-fusion (a) and b associated (b) modes with subsequent decay to τ lepton pairs. The median expected limits of the 2015 analysis [33] are indicated by the red line and the one and two sigma region by the green and yellow bands, respectively. Median expected limit projections are given for 300 fb^{-1} and 3000 fb^{-1} under three scenarios, as described in the text.

The projected model-dependent limits in the $m_{\mathrm{h}}^{\mathrm{mod+}}$ benchmark [34] are given in Fig. 11. The expected exclusion region of the 2015 analysis is indicated in pink, and the corresponding one- and two-sigma uncertainties as dark and light grey bands. The projected limits at 300 fb^{-1} and

3000 fb^{-1} are indicated by the blue and red dashed lines, respectively. In the results of the 2015 analysis the likelihood test used to determine the limits compares the presence of the three neutral MSSM Higgs bosons to the single SM Higgs boson. In MSSM benchmark scenarios like the $m_h^{\text{mod+}}$, there are small differences between the SM and MSSM predictions for the 125 GeV Higgs boson signal. For these projections only the presence of the two additional Higgs bosons H and A is tested, as comparing the SM and MSSM predictions for the 125 GeV Higgs boson would yield a complete, but unrealistic, exclusion of the m_A-tan β. As integrated luminosity increases and the properties of the 125 GeV Higgs boson are measured to increasingly high precision, such MSSM benchmarks are expected to be updated to retain consistency with the experimental observation.

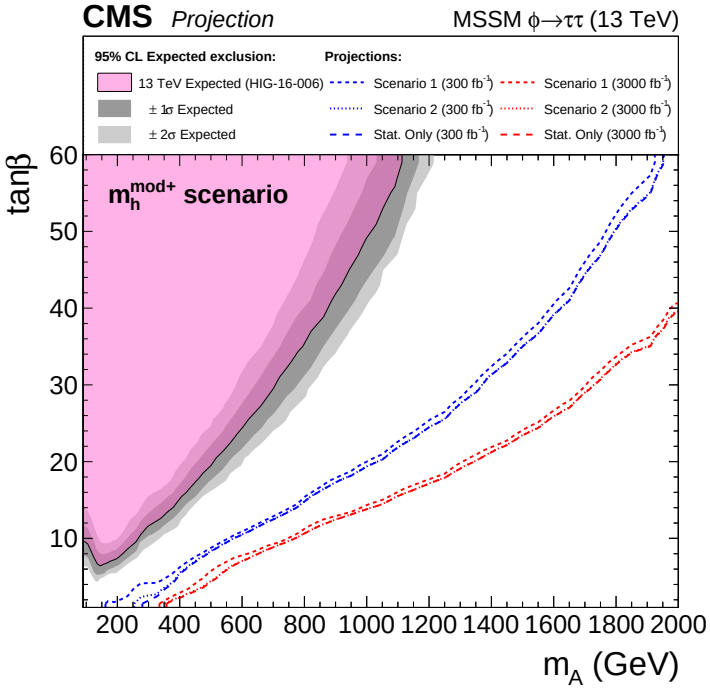

Figure 11: Projected 95% CL exclusion region in the MSSM $m_h^{\text{mod+}}$ benchmark scenario. The expected exclusion of the 2015 analysis [33] is given by the pink area and grey bands. The result compares the three neutral Higgs bosons, h, H and A, predicted in the MSSM to the single 125 GeV h in the SM. In order not to be sensitive to current differences in 125 GeV h prediction between the two, the projected limits do not include the h as part of the signal, thus the projected sensitivity is based solely on the expectation for H and A. Median expected exclusion projections are given for 300 fb^{-1} and 3000 fb^{-1} under three scenarios, as described in the text.

8 VBF H → invisible

The following result represents the extrapolation of the search for invisible decays of a Higgs boson produced via vector boson fusion performed in the 13 TeV data set collected by CMS in 2015 [35]. A previous upper limit on the Higgs invisible branching ratio at the HL-LHC had been performed in [5] and focused on the associated production with a Z boson.

The original data set corresponds to an integrated luminosity of 2.3 fb^{-1}. A dedicated trigger is used to select events with a jet pair compatible with vector boson fusion production of a Higgs

boson, together with missing transverse energy from its invisible decay. The offline selection makes further use of the event topology. Backgrounds arise from Z($\nu\nu$)+jets and W($l\nu$)+jets in which the charged lepton is unidentified, and QCD multijet production. Signal and background yields are extracted from a simultaneous fit to the signal region and multiple control regions. Minor backgrounds from diboson and top-quark processes are estimated from Monte Carlo simulation. The observed (expected) upper limit on the invisible branching fraction of the 125 GeV Higgs boson is found to be 69% (62%), assuming the SM production cross section. These upper limits improve to 24% (23%) when considering the combining the results of searches targeting production via gluon fusion, vector boson fusion, and in association with a vector boson, and combining with the 8 TeV data set.

Figure 12 shows the expected 95% upper limit on BR(H$\rightarrow$ inv.), for vector boson fusion production of a Higgs boson, as a function of integrated luminosity. The black solid line, labeled ECFA16 S1, corresponds to a scenario in which systematic uncertainties are fixed to the 2015 values. The red solid line, ECFA16 S2, corresponds to a scenario in which the experimental systematic uncertainties decrease with integrated luminosity until a lower bound based on the current understanding of the performance of the upgraded detector at 200 PU is reached, and theoretical uncertainties are scaled by 1/2 compared to the current values. Finally, the dashed green line shows a simple scaling with integrated luminosity of the experimental uncertainties, without a lower bound, and a 1/2 factor for the theoretical uncertainties. Table 7 shows the comparison for the 300 and 3000 fb^{-1} benchmark luminosities. These projections follow the analysis strategy described in [35], and do not consider further analysis improvements which could have a sizable impact in the sensitivity with the existing Run II data sample.

Table 7: The extrapolated 95% CL upper limit on the Higgs invisible branching ratio at 300 and 3000 fb^{-1} through the study of vector boson fusion production of the boson.

	ECFA2016 (S1)	ECFA2016 (S2+)	ECFA2016 (S2)
300 fb^{-1}	0.210	0.092	0.084
3000 fb^{-1}	0.200	0.056	0.028

9 Summary

The discovery of the Higgs boson opened a new era of precision measurements of the properties of the new particle, aimed to thoroughly test its consistence with the SM predictions. The present measurements of the Higgs boson couplings to fermions, bosons and of the tensor structure of the Higgs boson interaction with electroweak gauge bosons show no significant deviations with respect to the SM expectations. The HL-LHC will provide an unique environment in which to test the Higgs boson properties.

This summary describes Higgs boson analyses performed on the 13 TeV 2015 and early 2016 and projected to larger data sets of 300 and 3000 fb^{-1}. The projections are performed under different scenarios considering the systematic uncertainties in the present and in the HL-LHC conditions. The performance of H $\rightarrow$ ZZ, H $\rightarrow \gamma\gamma$, HH and BSM H $\rightarrow \tau\tau$, and H $\rightarrow$ inv. are shown. Further improvements of the sensitivity are expected when results based on larger data sets and using more sophisticated analysis techniques will be used for the projections.

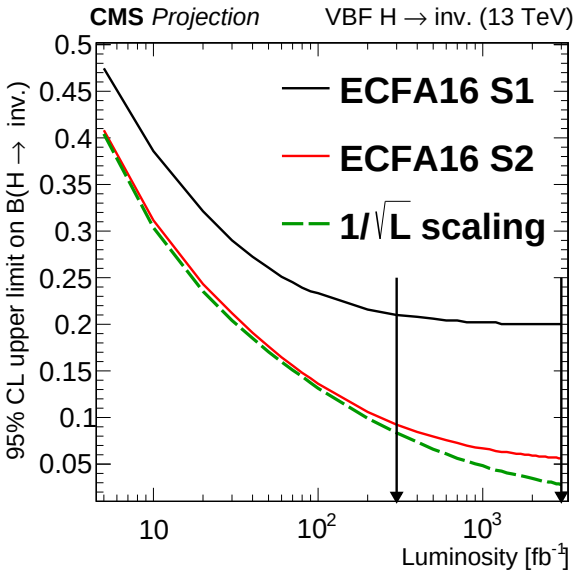

Figure 12: Expected 95% upper limit on BR(H→inv.) as a function of luminosity, for vector boson fusion production of a Higgs boson.

References

[1] ATLAS Collaboration, "Observation of a new particle in the search for the Standard Model Higgs boson with the ATLAS detector at the LHC", *Phys. Lett. B* **716** (2012) 129.

[2] CMS Collaboration, "Observation of a new boson at a mass of 125 GeV with the CMS experiment at the LHC", *Phys. Lett. B* **716** (2012) 3061.

[3] CMS Collaboration, "Observation of a new boson with mass near 125 GeV in pp collisions at $\sqrt{s}$ = 7 and 8 TeV", *JHEP* **06** (2013) 081, doi:10.1007/JHEP06(2013)081, arXiv:1303.4571.

[4] CMS Collaboration, "Technical Proposal for the Phase-II Upgrade of the CMS Detector", Technical Report CERN-LHCC-2015-010. LHCC-P-008. CMS-TDR-15-02, 2015.

[5] CMS Collaboration, "Projected Performance of an Upgraded CMS Detector at the LHC and HL-LHC: Contribution to the Snowmass Process", in *Proceedings, Community Summer Study 2013: Snowmass on the Mississippi (CSS2013): Minneapolis, MN, USA, July 29-August 6, 2013*. 2013. arXiv:1307.7135.

[6] DELPHES 3 Collaboration, "DELPHES 3, A modular framework for fast simulation of a generic collider experiment", *JHEP* **02** (2014) 57, doi:doi:10.1007/JHEP02(2014)057, arXiv:1307.6346.

[7] P. Fayet, "Supergauge invariant extension of the Higgs mechanism and a model for the electron and its neutrino", *Nucl. Phys. B* **90** (1975) 104 – 124, doi:http://dx.doi.org/10.1016/0550-3213(75)90636-7.

[8] P. Fayet, "Spontaneously broken supersymmetric theories of weak, electromagnetic and strong interactions", *Phys. Lett. B* **69** (1977), no. 4, 489 – 494, doi:http://dx.doi.org/10.1016/0370-2693(77)90852-8.

[9] LHC Higgs Cross Section Working Group Collaboration, "Handbook of LHC Higgs Cross Sections: 4. Deciphering the Nature of the Higgs Sector", arXiv:1610.07922.

[10] CMS Collaboration, "Updated measurements of Higgs boson production in the diphoton decay channel at $\sqrt{s} = 13$ TeV in pp collisions at CMS", CMS Physics Analysis Summary CMS-PAS-HIG-16-020, 2016.

[11] CMS Collaboration, "Initial Report of the Fast Timing Working Group", CMS Performance Note CMS-DP-2016-008, 2016.

[12] CMS Collaboration, "Measurements of properties of the Higgs boson and search for an additional resonance in the four-lepton final state at sqrt(s) = 13 TeV", CMS Physics Analysis Summary CMS-PAS-HIG-16-033, 2016.

[13] CMS Collaboration, "Constraints on the spin-parity and anomalous HVV couplings of the Higgs boson in proton collisions at 7 and 8 TeV", *Phys. Rev. D* **92** (2015) 012004, doi:10.1103/PhysRevD.92.012004, arXiv:1411.3441.

[14] CMS Collaboration, "Limits on the Higgs boson lifetime and width from its decay to four charged leptons", *Phys. Rev. D* **92** (2015), no. 7, 072010, doi:10.1103/PhysRevD.92.072010, arXiv:1507.06656.

[15] LHC Higgs Cross Section Working Group, "Handbook of LHC Higgs Cross Sections: 3. Higgs Properties", Yellow Report CERN-2013-004, 2013.

[16] CMS Collaboration, "Search for H(bb)H($\gamma\gamma$) decays at 13 TeV", CMS Physics Analysis Summary CMS-PAS-HIG-16-032, 2016.

[17] CMS Collaboration, "Search for non-resonant Higgs boson pair production in the $\mathrm{b\bar{b}}\tau^+\tau^-$ final state", CMS Physics Analysis Summary CMS-PAS-HIG-16-012, 2016.

[18] CMS Collaboration, "Search for non-resonant pair production of Higgs bosons in the $\mathrm{b\bar{b}b\bar{b}}$ final state with 13 TeV CMS data", CMS Physics Analysis Summary CMS-PAS-HIG-16-026, 2016.

[19] CMS Collaboration, "Search for Higgs boson pair production in the $\mathrm{b\bar{b}}l\nu l\nu$ final state at $\sqrt{s} = 13$ TeV", CMS Physics Analysis Summary CMS-PAS-HIG-16-024, 2016.

[20] CMS Collaboration, "Search for two Higgs bosons in final states containing two photons and two bottom quarks in proton-proton collisions at 8 TeV", *Phys. Rev. D* **94** (2016) doi:10.1103/PhysRevD.94.052012, arXiv:1603.06896.

[21] CMS Collaboration Collaboration, "Higgs pair production at the High Luminosity LHC", Technical Report CMS-PAS-FTR-15-002, CERN, Geneva, 2015.

[22] CMS Collaboration, "Search for resonant pair production of Higgs bosons decaying to two bottom quark-antiquark pairs in proton-proton collisions at 13 TeV", CMS Physics Analysis Summary CMS-PAS-HIG-16-002, 2016.

[23] L. Randall and R. Sundrum, "A Large mass hierarchy from a small extra dimension", *Phys. Rev. Lett.* **83** (1999) 33703373.

[24] W. D. Goldberger and M. S. Wise, "Modulus stabilization with bulk fields", *Phys. Rev. Lett.* **83** (1999) 49224925.

[25] O. DeWolfe, D. Freedman, S. Gubser, and A. Karch, "Modeling the fifth-dimension with scalars and gravity", *Phys. Rev. D* **62** (2000) 046008.

[26] C. Csaki, M. Graesser, L. Randall, and J. Terning, "Cosmology of brane models with radion stabilization", *Phys. Rev. D* **62** (2000) 045015.

[27] C. Csaki, J. Hubisz, and S. J. Lee, "Radion phenomenology in realistic warped space Model", *Phys. Rev. D* **76** (2007) 125015.

[28] G. F. Giudice, R. Rattazzi, and J. D. Wells, "Graviscalars from higher-dimensional metrics and curvature-Higgs mixing", *Nucl. Phys. B* **595** (2001) 250, doi:10.1016/S0550-3213(00)00686-6, arXiv:hep-ph/0002178.

[29] GEANT4 Collaboration, "GEANT4: A Simulation toolkit", *Nucl. Instrum. Meth. A* **506** (2003) 250.

[30] CMS Collaboration, "Study of Pileup Removal Algorithms for Jets", CMS Physics Analysis Summary CMS-PAS-JME-14-001, 2014.

[31] D. Bertolini, H. P., M. Low, and N. Tran, "Pileup per particle identification", *JHEP* **10** (2014) 59, doi:doi:10.1007/JHEP10(2014)059, arXiv:1407.6013.

[32] G. de Florian and J. Mazzitelli, "Higgs Boson Pair Production at Next-to-Next-to-Leading Order in QCD", *Phys. Rev. Lett.* **111** (2013) 201801, doi:doi:10.1103/PhysRevLett.111.201801, arXiv:1309.6594.

[33] CMS Collaboration, "Search for a neutral MSSM Higgs boson decaying into $\tau\tau$ at 13 TeV", CMS Physics Analysis Summary CMS-PAS-HIG-16-006, 2016.

[34] M. Carena et al., "MSSM Higgs Boson Searches at the LHC: Benchmark Scenarios after the Discovery of a Higgs-like Particle", *Eur. Phys. J.* **C73** (2013), no. 9, 2552, doi:10.1140/epjc/s10052-013-2552-1, arXiv:1302.7033.

[35] CMS Collaboration, "Searches for invisible Higgs boson decays with the CMS detector", CMS Physics Analysis Summary CMS-PAS-HIG-16-016, 2016.